GSA Data Repository 2017132

Tobias Grützner, Stephan Klemme, Arno Rohrbach, Fernanda Gervasoni, and Jasper Berndt, 2017, The role of F-clinohumite in volatile recycling processes in subduction zones: Geology, doi:10.1130/G38788.1.

Supplementary data

MATERIALS AND METHODS

Starting Materials

Starting materials were prepared from analytical MgO, SiO_2, MgF_2 and $Mg(OH)_2$. To release absorbed water and unwanted hydroxide components, the MgO starting material was fired in a Pt-crucible at 1000°C for at least 2 h. The starting materials were ground in an agate mortar under acetone (>1 h) to obtain homogenous fine grained mixtures. All starting materials including the fired MgO were stored in a drying furnace at >110°C to prevent the mixtures from absorbing moisture.

Experimental techniques

All experiments were performed in sealed 2 mm O.D. Pt-capsules to prevent volatile loss. In our low pressure experiments, F partially volatilizes and forms a gas phase which reduces the F activity in the melt and causes excess MgO in the melts (Hinz & Knuth, 1960). Two experiments were conducted at atmospheric pressure (1 atm) in a vertical gas-mixing furnace (Gero GmbH, Germany) at temperatures between 1350-1500°C (Table DR1). Experiments at pressures between 0.5 -2 GPa and at 1350°C<T<1600°C were conducted in Boyd & England type piston cylinder apparatus at Münster University. The ½ inch piston cylinder assemblies consisted of concentric cylinders of talc, Duran© glass, a thin graphite heater (Ringsdorff©), and a 4 mm diameter inner cylinder made from crushable alumina. The temperatures were monitored with a $W_{97}Re_3$-$W_{75}Re_{25}$ thermocouple and controlled by a Eurotherm™-controller. The temperatures were accurate within 10°C. The pressure assemblies were calibrated using the quartz–coesite transition (Bose & Ganguly, 1995) and the $MgCr_2O_4$+SiO_2 =

$MgSiO_3$+Cr_2O_3 reaction (Klemme & O'Neill, 1997). Based on our pressure calibration, the quoted pressures are estimated to be accurate within 0.1 GPa.

Experiments at pressures between 5 GPa and 19 GPa were run in a 1000 t Walker-type (Walker *et al.*, 1990) multi-anvil apparatus at Münster University. Experiments from 5 to 8 GPa were performed with 14/8 assemblies, experiments at 17 and 19 GPa with 10/4 assemblies. The 14/8 and 10/4 notation refers to octahedra size and truncated edge lengths in mm. All multi-anvil assemblies consist of Cr-bearing MgO octahedra, stepped $LaCrO_3$ heaters and pyrophyllite gaskets (Wonderstone Ltd). The starting materials were sealed in Pt capsules, encapsulated into crushable Al_2O_3 containers and finally placed in the center of the furnace. We used one 1.6 mm O.D. Pt-capsule with a length of about 2.7 mm in the 14/8 assemblies and two 1.2 mm O.D. Pt-capsules with a length of 1.2 mm for the 10/4 assemblies. Temperatures were measured with $W_{97}Re_3$-$W_{75}Re_{25}$ thermocouples and were inserted on top of the capsules (for the 14/8 assemblies) or centered between the two capsules (for 10/4 assemblies). First, the pressure was applied using a computer-controlled system and subsequently experiments were heated up fast with about 300°C/min and then kept constant for 1-5 h (Table DR1). Temperatures were controlled by a Eurotherm™ 2404 - controller. The temperatures measured at the thermocouples were accurate within 10°C. All experiments were quenched rapidly by turning off the power supply. Temperature fell from the run temperature to below 500°C in less than 1 s.

Run M-92 at 17 GPa and 1900°C seems to violate Gibb's phase rule. This is caused by a large temperature gradient of about 100 °C in this particular experiment and is a common challenge in the most very high temperature multi anvil experiments (Stewart *et al.*, 2007; Leinenweber *et al.*, 2012). As the thermocouple is located in the center of the 10/4 assembly between two capsules, the measured temperature defines the upper limit of the T gradient. The characterization of the run with SEM imaging analyses confirms that the humite group minerals are concentrated at the cold end of the capsule, whereas forsterite, enstatite and melt are concentrated at the hot end of the capsule. Temperature gradients might also explain the small number of clinohumites found in run M-117,

which are only located at the cold end of the capsule and are, therefore, not be stable at the nominal run temperature of 1700°C.

Analytical Methods

The experimental run products were characterized first by optical microscopy, followed by scanning electron microscopy, using JEOL 6610LV scanning electron microscope which is equipped with an EDX detector (Fig. DR1). To quantify major element concentrations of the experimental products, a JEOL JXA 8900 electron microprobe (EPMA) was used (Table DR2). Measurement conditions were typically 15 kV acceleration voltage, 5 nA beam current and 10 µm beam diameter. Fluorine concentrations of all phases were analyzed with a synthetic multi-layered diffraction crystal (LDE). Counting times were 20 s on the peak and 10 s on the background for all elements.

In sample M-114, M-116 and M117 oxygen concentrations were measured using a LDE crystal at the aforementioned conditions. Water in all runs was then calculated using excess oxygen.

Raman spectroscopy measurements were performed at the Institute for Physical Chemistry in Münster, using a Jobin-Yvon LabRam HR800 spectrometer with a 532 nm wavelength laser, a focal length of 200mm and a diffraction grating of 1800 gr/mm (Fig. DR2). After using a Si standard for calibration, the spectra were obtained by averaging two spectra with an acquisition time of 30-40s for shift ranges of 150 to 1800 cm^{-1}.

The influence of Ti and Fe on clinohumite stability in subduction zones

Our data show F-clinohumite is much more stable than its OH-bearing endmembers. This implies that F-clinohumite should also be stable at high temperatures in a more complex, i.e. in compositions close to natural systems. The most important additional chemical components in natural clinohumites are Fe and Ti (e.g. Aoki & Akaogi, 1976; Gaspar, 1992; Weiss, 1997; Koga et al., 2014). However, it is well known that the addition of Fe to the system will lower the temperature stability of clinohumite only very slightly (Iwamori, 2004). On the other hand, natural clinohumite containts

often high concentrations of Ti (e.g. Evans & Trommsdorff, 1983; López Sánchez-Vizcaíno et al., 2005) and it has been shown that Ti, very much like F, stabilizes clinohumite to higher temperatures (e.g. Weiss, 1997; Stalder & Ulmer, 2001; Koga et al., 2014). However, it is also known that Ti and F tend to exclude each other (Evans & Trommsdorff, 1983; Ribbe et al., 1968). Consequently, Evans & Trommsdorff (1983) describe natural clinohumites with varying amounts of Ti (X_{Ti} = 0-0.4) and F (X_F = 0.1-0.45), where both elements correlate inversely. A pioneering study from Ribbe et al. (1968) suggests that Ti has a destabilizing effect on the clinohumite structure, which limits the natural content to about 0.5 cations per formula unit (X_{Ti} = 0.5). Weiss (1997) and Ulmer & Trommsdorff (1999) show that Ti-saturated OH-clinohumite with X_{Ti} = 0.46 is stable at T well above the choke point (Figure 1 – line [A]), but these Ti-rich clinohumites are less stable than Ti-free OH-clinohumite with small amounts of fluorine of X_{Ti} < 0.1 (Figure 1 – line [B]). We can therefore safely assume that the F in clinohumite plays the dominant role on the stability of clinohumite in subduction zones.

REFERENCES

Aoki, K.-i., Fujino, K., and Akaogi, M., 1976, Titanochondrodite and titanoclinohumite derived from the upper mantle in the Buell Park Kimberlite, Arizona, USA: Contributions to Mineralogy and Petrology, v. 56, no. 3, p. 243–253, doi: 10.1007/BF00466824.

Bose, K., and Ganguly, J., 1995, Quartz-coesite transition revised: Reversed experimental determination at 500-1200 °C retrieved thermochemical properties: American Mineralogist, v. 80, p. 231–238.

Evans, B.W., and Trommsdorff, V., 1983, Fluorine hydroxyl titanian clinohumite in alpine recrystallized garnet peridotite: compositional controls and petrologic significance: American Journal of Science, 283-A, p. 355–369.

Gaspar, J.C., 1992, Titanian clinohumite in the carbonatites of the Jacupiranga Complex, Brazil: Mineral chemistry and comparison with titanian clinohumite from other enviroments: American Mineralogist, v. 77, p. 168–178.

98 Hauri, E.H., 2002, SIMS analysis of volatiles in silicate glasses, 2: isotopes and abundances in Hawaiian
99 melt inclusions: Chemical Geology, v. 183, p. 115–141.
100 Hervig, R.L., and Bell, D.R., 2005, Fluorine and hydrogen in mantle megacrysts: American Geophysical
101 Union Fall meeting, p. V41A-1426.
102 Hinz, W., and Knuth, P.O., 1960, Phase equilibrium data for the system MgO-MgF_2-SiO_2: American
103 Mineralogist, v. 45, p. 1198–1210.
104 Iwamori, H., 2004, Phase relations of peridotites under H_2O-saturated conditions and ability of
105 subducting plates for transportation of H_2O: Earth and Planetary Science Letters, v. 227, 1-2, p.
106 57–71.
107 Klemme, S., and O'Neill, H.S.C., 1997, The reaction $MgCr_2O_4 + SiO_2 = Cr_2O_3 + MgSiO_3$ and the free
108 energy of formation of magnesiochromite ($MgCr_2O_4$): Contributions to Mineralogy and Petrology,
109 v. 130, p. 59–65.
110 Klemme, S., 2004, Evidence for fluoride melts in Earth's mantle formed by liquid immiscibility:
111 Geology, v. 32, no. 5, p. 441.
112 Koga, K.T., Garrido, C.J., Padrón-Navarta, J.A., Sánchez-Vizcaíno, V., and Gómez-Pugnaire, M.T., 2014,
113 FTIR and Raman spectroscopy characterization of fluorine-bearing titanian clinohumite in
114 antigorite serpentinite and chlorite harzburgite: Earth, Planets and Space, v. 66.
115 Leinenweber, K.D., Tyburczy, J.A., Sharp, T.G., Soignard, E., Diedrich, T., Petuskey, W.B., Wang, Y., and
116 Mosenfelder, J.L., 2012, Cell assemblies for reproducible multi-anvil experiments (the COMPRES
117 assemblies): American Mineralogist, v. 97, 2-3, p. 353–368.
118 López Sánchez-Vizcaíno, V., Trommsdorff, V., Gómez-Pugnaire, M.T., Garrido, C.J., Müntener, O., and
119 Connolly, J.A.D., 2005, Petrology of titanian clinohumite and olivine at the high-pressure
120 breakdown of antigorite serpentinite to chlorite harzburgite (Almirez Massif, S. Spain):
121 Contributions to Mineralogy and Petrology, v. 149, no. 6, p. 627–646.
122 Lyubetskaya, T., and Korenaga, J., 2007, Chemical composition of Earth's primitive mantle and its
123 variance: 1. Method and results: Journal of Geophysical Research, v. 112, B3, p. B03211.

124 Palme, H., and O'Neill, H.S.C., 2003, Cosmochemical Estimates of Mantle Composition, in Holland,
125 H.D., Turekian, K.K., eds., Treatise on geochemistry, First edition ed.: Amsterdam, Boston,
126 Elsevier, p. 1–38.
127 Pyle, D., and Mather, T., 2009, Halogens in igneous processes and their fluxes to the atmosphere and
128 oceans from volcanic activity: A review: Chemical Geology, v. 263, 1-4, p. 110–121.
129 Ribbe, P.H., Gibbs, G.V., and Jones, N.W., 1968, Cation and anion substitutions in the humite
130 minerals: Mineralogical Magazine, v. 36, p. 283–966.
131 Saal, A.E., Hauri, E.H., Langmuir, C.H., and Perfit, M.R., 2002, Vapour undersaturation in primitive
132 mid-ocean-ridge basalt and the volatile content of Earth's upper mantle: Nature, v. 419, p. 451–
133 455.
134 Salters, Vincent J. M., and Stracke, A., 2004, Composition of the depleted mantle: Geochemistry,
135 Geophysics, Geosystems, v. 5, no. 5, p. Q05004, doi: 10.1029/2003GC000597.
136 Stalder, R., and Ulmer, P., 2001, Phase relations of a serpentine composition between 5 and 14 GPa:
137 significance of clinohumite and phase E as water carriers into the transition zone: Contributions
138 to Mineralogy and Petrology, v. 140, no. 6, p. 670–679.
139 Stewart, A.J., van Westrenen, W., Schmidt, M.W., and Melekhova, E., 2007, Effect of gasketing and
140 assembly design: A novel 10/3.5 mm multi-anvil assembly reaching perovskite pressures: High
141 Pressure Research, v. 26, no. 3, p. 293–299, doi: 10.1080/08957950600835237.
142 Trommsdorff, V., and Evans, B.W., 1980, Titanian Hydroxyl-Clinohumite: Formation and Breakdown
143 in Antigorite Rocks (Malenco, Italy): Contributions to Mineralogy and Petrology, v. 72, p. 229–
144 242.
145 Walker, D., Carpenter, M.A., and Hitch, C.M., 1990, Some simplifications to multianvil devices for
146 high pressure experiments: American Mineralogist, v. 75, p. 1020–1028.
147 Weiss, M., 1997, Clinohumites, a field and experimental study [[Ph.D. thesis]: Zürich, ETH, 168 p.
148

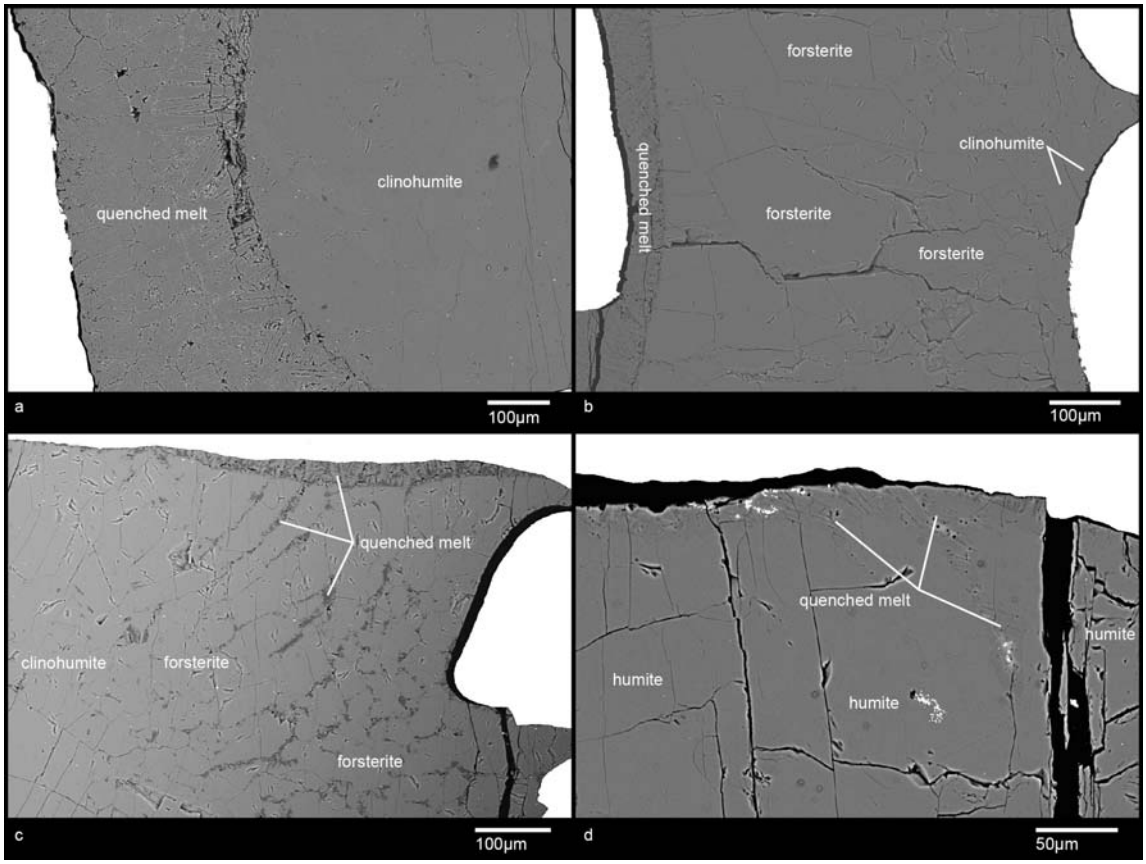

Figure DR1 Representative backscattered electron images of experimental run products. a) M-65, b) M-117, c) M-116, d) M-121. Phases were determined using Raman Spectroscopy and EPMA.

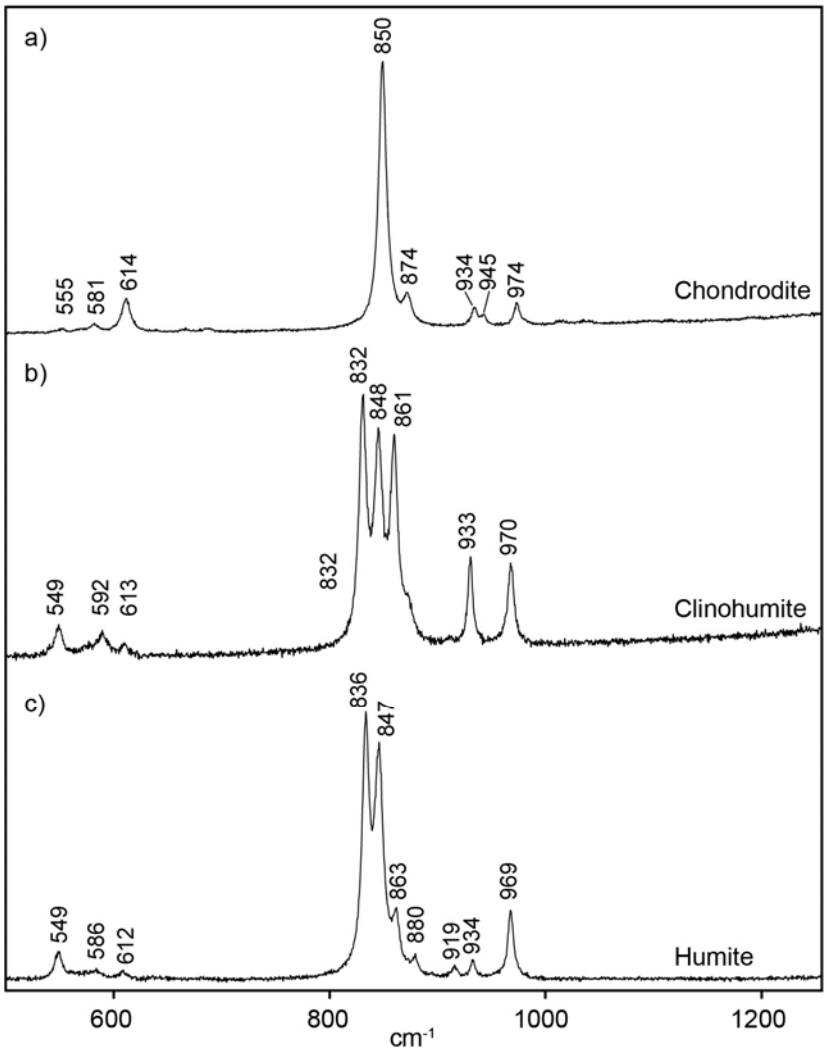

153

154 Figure DR2 Raman spectra of a) F-chondrodite (M-122), b) F-clinohumite (M-65) and c) F-Humite

155 (M-122).

156

157 Table DR1 Experimental runs, 1 atm=atmospheric pressure, chn = chondrodite,
158 chu=clinohumite, en=enstatite, hu = humites, fo=forsterite, melt=quenched melt, per= periclase, wd
159 = wadsleyite, ahyB = anhydrous B.

Run	T (°C)	P (GPa)	Run time (h)	Present phases
Starting Material: 6 MgO, 3 SiO_2, 1 MgF_2 (mol proportion)				
M-33	1300	1 atm	48	chu+per
M-13	1500	1 atm	96	fo+melt
M-122	1350	1	4	chn, chu, hu
M-12	1500	1	4	fo+melt
M-121	1500	2	4	hu+melt
M-120	1600	2	2	fo +melt
M-65	1500	5	2	chu+melt
M-82	1700	6	4	fo+chu+melt
M-111	1800	6	0.3	fo+melt?
M-24	1500	8,0	4	chu+en
M-83	1700	17	4	hu+chn+en
M-92	1900	17	0.5	fo+en+hu+chu+chn
M-99	1500	19	3	wd+chn
M-97	1700	19	2	wd+melt
Starting Material: 6 MgO, 3 SiO_2, 0.5 MgF_2, 0.5 $Mg(OH)_2$ (mol proportion)				
M-114	1400	10	2	chu+fluid
M-116	1600	10	1	chu+fo+melt+fluid
M-117	1700	10	1	fo(+chu)+melt+fluid

160

161 Table DR2 Representative oxide, F and OH concentrations analyzed with EPMA techniques (wt%). *Number of analyses given in brackets

162 after the run number. Uncertainties are given in the brackets after the analysis, b.d.= below detection limit.

Experiment (#)*	**F**	**OH**	**SiO_2**	**MgO**	**FeO**	**Al_2O_3**	**CaO**	**TiO_2**	**Total**
F-Chondrodite									
M-24 (6)	9.9(3)	-	34.5(3)	58.4(2)	0.04(2)	0.03(1)	0.06(2)	0.04(2)	98.8(3)
F-Clinohumite									
M-65 (20)	5.9(7)	-	37.7(5)	58.4(3)	b.d	b.d	0.03(1)	b.d	99.7(3)
M-92 (2)	6.2	-	37.5	57.7	b.d.	0.07	b.d.	0.04	98.9
F-Humite									
M-92 (1)	7.9	-	36.87	58.2	b.d.	0.05	0.05	0.08	99.8
M-122(31)	8.5(4)		37.2(4)	57.6(4)	b.d.	0.2(2)	b.d.	b.d.	99.8(5)
Clinohumite, 50mol% F^-, 50mol% OH^-									
M-116 (11)	3.7(2)	2.3(6)	37.7(2)	58.3(3)	b.d.	0.27(3)	b.d.	b.d.	99.5(3)
M-114 (7)	3.4(3)	1.3(5)	38.2(1)	58.3(1)	b.d.	0.17(4)	b.d.	b.d.	99.2(4)
M-117 (3)	4.6(3)	2.6(7)	37.4(1)	58.2(2)	b.d.	0.22(2)	b.d.	b.d.	99.7(2)

163